2D DOA Estimation of Coherent Signals Exploiting Moving Uniform Rectangular Array

Saidur R. Pavel and Yimin D. Zhang, *Fellow, IEEE*

***Abstract*—This letter considers two-dimensional direction of arrival (DOA) estimation of coherent signals exploiting a moving uniform rectangular array. The motion of the array induces phase variations in the received signals across spatial positions, enabling the construction of decorrelated covariance matrices through forward-backward spatial smoothing. We analyze the achievable degrees of freedom (DOFs) in terms of movement steps and examine the impact of the motion support on effective decorrelation. Notably, we show that the maximum number of DOFs can be achieved if each movement step is at least half the signal wavelength and the number of movement steps is no less than half the number of array elements. Furthermore, it is demonstrated that distributing motion across both array axes yields better decorrelation and estimation performance than restricting movement to a single dimension.**

***Index Terms*—Coherent signals, direction of arrival (DOA) estimation, moving array, spatial smoothing.**

I. Introduction

DIRECTION of arrival estimation (DOA) estimation is a fundamental research area in array signal processing, with broad applications in radar, sonar, and wireless communications [1], [2], [3], [4], [5], [6], [7]. Commonly used subspace-based methods, such as MUSIC [8] and ESPRIT [9], are developed under the assumption of uncorrelated sources to ensure full-rank covariance matrix. When the sources are fully or partially correlated, the covariance matrix becomes rank-deficient. In such cases, a rank-restoration or decorrelation technique is required to recover the full-rank structure of the covariance matrix and enable subspace-based DOA estimation [10], [11], [12], [13], [14], [15].

Spatial smoothing [10], [11], [12], which partitions a full array into multiple overlapping subarrays, is a commonly technique used to decorrelate coherent signals. For an N-element uniform linear array (ULA), this method can achieve a maximum of $\lfloor \frac{N}{2} \rfloor$ degrees of freedom (DOFs), where $\lfloor \cdot \rfloor$ denotes the floor function. Forward-backward spatial smoothing, introduced in [16], increases the DOFs to $\lfloor \frac{2}{3}N \rfloor$. A computationally efficient alternative that avoids explicit spatial smoothing was proposed in [17], and its forward-backward extension was subsequently presented in [18]. In [19], a Toeplitz reconstruction-based method was developed to handle mixed coherent and uncorrelated signals. These techniques are primarily developed for linear arrays, restricting DOA estimation to one dimension, typically azimuth. However, many practical applications require two-dimensional (2D) DOA estimation involving both azimuth and elevation angles. A 2D spatial smoothing technique for uniform rectangular arrays (URAs) was proposed in [20], and its forward-backward variation in [21], but both offer a limited number of DOFs.

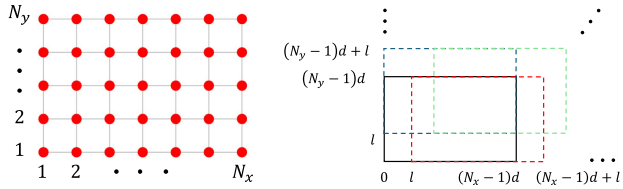

(a) Array configuration (b) Moving URA

Fig. 1. URA configuration and moving URA concept.

Unlike spatial smoothing based on static arrays, moving array platforms can achieve an increased synthetic aperture by combining data from the original array and its spatially shifted versions, assuming stationary or slowly time-varying signal environments [22], [23], [24], [25], [26], [27], [28]. DOA estimation is studied in [29] for a coprime array with a constant velocity. Forward-backward spatial smoothing across different array positions yields a decorrelated covariance matrix for coherent signals.

In this letter, we address 2D DOA estimation of coherent signals using an $N_x \times N_y$ URA. By moving the URA along both array axes, phase variations are introduced across different array positions, thus enabling motion-enabled smoothing that achieves significantly higher DOFs compared to static arrays. We show that the full array DOFs are attainable when the array undergoes at least $(N_xN_y-1)/2$ movement steps, with each step being equal to or greater than half a wavelength. We analyze the effect of different motion supports on signal decorrelation, which is unique to the 2D array configuration because the array can move along a single axis (either X or Y), or follow a zig-zag trajectory covering both dimensions. We demonstrate that motion along both axes provides better decorrelation performance than one-dimensional movement due to diversified 2D phase variation. Theoretical analysis and simulations validate the proposed framework.

Received 16 November 2025; accepted 14 December 2025. Date of publication 19 December 2025; date of current version 30 December 2025. This work was supported in part by the National Science Foundation (NSF) under Grant ECCS-2236023 and in part by the Air Force Office of Scientific Research (AFOSR) under Grant FA9550-23-1-0255. The associate editor coordinating the review of this article and approving it for publication was Dr. Hua Chen. *(Corresponding author: Yimin D. Zhang.)*

The authors are with the Department of Electrical and Computer Engineering, Temple University, Philadelphia, PA 19122 USA (e-mail: pavel.saidur@temple.edu; ydzhang@temple.edu).

Digital Object Identifier 10.1109/LSP.2025.3646141

Notations: Lower-case bold letters and upper-case bold letters are used to denote vectors and matrices, respectively. Specifically, $\boldsymbol{I}$ represents the identity matrix of appropriate dimensions. Operators $(\cdot)^{\mathrm{T}}$, $(\cdot)^*$, and $(\cdot)^{\mathrm{H}}$ denote the transpose, complex conjugate, and Hermitian of a matrix or vector, respectively. The operator $\mathrm{Diag}(\cdot)$ forms a diagonal matrix from a vector, whereas $\mathrm{diag}(\cdot)$ extracts the diagonal elements of a matrix as a vector. In addition, $\mathbb{C}^{M\times N}$ denotes the space of $M \times N$ complex-valued matrices, $[.]_k$ denotes kth entry of a vector, and $\mathbb{E}[\cdot]$ denotes the statistical expectation operator.

II. Signal Model

Consider a URA comprising N_x and N_y antennas along the X and Y axes as depicted in Fig. 1(a). The total number of antennas is therefore $N = N_xN_y$. K far-field narrowband coherent signals impinge on the array with DOAs $(\boldsymbol{\phi}, \boldsymbol{\theta})$, where $\boldsymbol{\phi} = [\phi_1, \phi_2, \ldots, \phi_K]^{\mathrm{T}}$ represents the azimuth angles and $\boldsymbol{\theta} = [\theta_1, \theta_2, \ldots, \theta_K]^{\mathrm{T}}$ represents the elevation angles. The baseband received array signal vector at time t is expressed as

$$\boldsymbol{x}(t) = \sum_{k=1}^{K} s_k \left(\boldsymbol{a}(\mu_k) \otimes \boldsymbol{a}(\nu_k)\right) + \boldsymbol{n}(t) = \boldsymbol{A}\boldsymbol{s}(t) + \boldsymbol{n}(t), \tag{1}$$

where $\boldsymbol{a}(\mu_k) = [1, e^{-j\frac{2\pi}{\lambda}d\mu_k}, \ldots, e^{-j\frac{2\pi}{\lambda}(N_x-1)d\mu_k}]^{\mathrm{T}} \in \mathbb{C}^{N_x}$ and $\boldsymbol{a}(\nu_k) = [1, e^{-j\frac{2\pi}{\lambda}d\nu_k}, \ldots, e^{-j\frac{2\pi}{\lambda}(N_y-1)d\nu_k}]^{\mathrm{T}} \in \mathbb{C}^{N_y}$ are the steering vectors along the X and Y directions corresponding to DOA (ϕ_k, θ_k), respectively, with $\mu_k = \sin(\theta_k)\cos(\phi_k)$ and $\nu_k = \sin(\theta_k)\sin(\phi_k)$, and $\boldsymbol{n}(t) \sim \mathcal{CN}(\boldsymbol{0}, \sigma_n^2\boldsymbol{I})$ is a zero-mean additive white Gaussian noise vector with noise power σ_n^2. In (1), $d = \lambda/2$ and λ is the wavelength. In addition, $\boldsymbol{A} = [\boldsymbol{a}(\mu_1) \otimes \boldsymbol{a}(\nu_1), \ldots, \boldsymbol{a}(\mu_K) \otimes \boldsymbol{a}(\nu_K)]$ is the array manifold matrix, and $\boldsymbol{s}(t) = [s_1(t), \ldots, s_K(T)]^{\mathrm{T}}$ denotes the signal waveform vector.

We consider the waveform corresponding to the DOA (ϕ_1, θ_1), i.e., $s_1(t)$, as the reference. Accordingly, the waveform associated with the kth coherent DOA is given by $s_k(t) = \alpha_k s_1(t)$ for $k = 1, 2, \ldots, K$ with $\alpha_1 = 1$. As such, the signal waveform vector becomes $\boldsymbol{s}(t) = s_1(t)\boldsymbol{\alpha}$, where $\boldsymbol{\alpha} = [\alpha_1, \alpha_2, \ldots, \alpha_K]^{\mathrm{T}}$ is the complex scaling vector for the coherent signals. The covariance matrix of the received signal vector becomes

$$\boldsymbol{R} = \mathbb{E}\left[\boldsymbol{x}(t)\boldsymbol{x}^{\mathrm{H}}(t)\right] = \sigma_s^2\boldsymbol{A}\boldsymbol{\alpha}\boldsymbol{\alpha}^{\mathrm{H}}\boldsymbol{A}^{\mathrm{H}} + \sigma_n^2\boldsymbol{I}, \tag{2}$$

where $\sigma_s^2 = \mathbb{E}[s_1(t)s_1^*(t)]$ is the signal power of the reference signal. Because all signals are coherent, the covariance matrix is rank 1. Therefore, it needs to be decorrelated for DOA estimation using subspace-based methods.

III. Decorrelation of Covariance Matrix Exploiting Moving Array

Now consider that the URA moves in a discrete stepwise manner. For each step, it moves by a fixed distance l along either the X or the Y direction, but not both simultaneously. In this way, the total displacement after p movements along the X direction and q movements along the Y direction becomes pl and ql, respectively, and the array position is denoted as (p, q). The array moves through a total of PQ positions.

Denote the antenna locations at the (p, q)th position as

$$\begin{aligned}\mathbb{S}_{p,q} = \{&(x_{\mathbb{S}}, y_{\mathbb{S}}) | x_{\mathbb{S}} \in [pl, (N_x-1)d + pl], \\ &y_{\mathbb{S}} \in [ql, (N_y-1)d + ql]\},\end{aligned} \tag{3}$$

where $p = 0, 1, \ldots, P-1$ and $q = 0, 1, \ldots, Q-1$ are the step indices along the X and Y directions, respectively. At array position (p, q), the array manifold matrix becomes

$$\boldsymbol{A}_{p,q} = \boldsymbol{A}\boldsymbol{\Phi}_{p,q}, \tag{4}$$

where $\boldsymbol{A}$ is the reference array manifold at array position $(0, 0)$, and $\boldsymbol{\Phi}_{p,q} = \mathrm{Diag}(\boldsymbol{\phi}_{p,q})$ with $\boldsymbol{\phi}_k = [e^{-j\gamma_{p,q}^1}, e^{-j\gamma_{p,q}^2}, \ldots, e^{-j\gamma_{p,q}^K}]$ and $\gamma_{p,q}^k = \frac{2\pi}{\lambda}l(p\mu_k + q\nu_k)$. We consider the varying-correlation case during the motion, i.e., the complex scaling vector $\boldsymbol{\alpha}$ may differ at each moving step. We denote by $\boldsymbol{\alpha}_{p,q}$ the scaling vector at array position (p, q). The received signal vector at array position (p, q) is expressed as

$$\boldsymbol{x}_{p,q}(t) = \boldsymbol{A}_{p,q}\boldsymbol{s}(t) = \boldsymbol{A}\boldsymbol{\Phi}_{p,q}\boldsymbol{s}(t). \tag{5}$$

The forward covariance matrix corresponding to array position (p, q) can be expressed as

$$\boldsymbol{R}_{p,q}^{(f)} = \sigma_s^2\boldsymbol{A}\boldsymbol{\Phi}_{p,q}\boldsymbol{\alpha}_{\boldsymbol{p},\boldsymbol{q}}\boldsymbol{\alpha}_{\boldsymbol{p},\boldsymbol{q}}{}^{\mathrm{H}}\boldsymbol{\Phi}_{p,q}^{\mathrm{H}}\boldsymbol{A}^{\mathrm{H}} + \sigma_n^2\boldsymbol{I}. \tag{6}$$

To obtain a decorrelated representation, we average the covariance matrices across all PQ positions to construct the forward spatially smoothed covariance matrix, given as

$$\boldsymbol{R}^{(f)} = \frac{1}{PQ}\sum_{p=0}^{P-1}\sum_{q=0}^{Q-1}\boldsymbol{R}_{p,q}^{(f)} = \boldsymbol{A}\boldsymbol{M}^{(f)}\boldsymbol{A}^{\mathrm{H}}, \tag{7}$$

where

$$\boldsymbol{M}^{(f)} = \frac{\sigma_s^2}{PQ}\sum_{p=0}^{P-1}\sum_{q=0}^{Q-1}\boldsymbol{c}_{p,q}\boldsymbol{c}_{p,q}^{\mathrm{H}} = \frac{\sigma_s^2}{PQ}\boldsymbol{C}\boldsymbol{C}^{\mathrm{H}} \tag{8}$$

with $\boldsymbol{c}_{p,q} = \boldsymbol{\Phi}_{p,q}\boldsymbol{\alpha}_{p,q} = \boldsymbol{D}_{p,q}\boldsymbol{\phi}_{p,q}$, where $\boldsymbol{D}_{p,q} = \mathrm{Diag}(\boldsymbol{\alpha}_{p,q})$ and $\boldsymbol{C} = [\boldsymbol{c}_{0,0}, \boldsymbol{c}_{0,1}, \ldots, \boldsymbol{c}_{P,Q}] \in \mathbb{C}^{K\times PQ}$.

Similarly, to perform backward smoothing, we also obtain a covariance matrix corresponding to the flipped and conjugated version of the received array signal vector at each array position (p, q), given as

$$\boldsymbol{R}_{p,q}^{(b)} = \sigma_s^2\boldsymbol{A}\boldsymbol{\Phi}_{p,q}\boldsymbol{\Phi}_{p,q}^{(b)}\boldsymbol{\alpha}_{p,q}^*\boldsymbol{\alpha}_{p,q}^{\mathrm{T}}(\boldsymbol{\Phi}_{p,q}^{(b)})^{\mathrm{H}}\boldsymbol{\Phi}_{p,q}^{\mathrm{H}}\boldsymbol{A}^{\mathrm{H}} + \sigma_n^2\boldsymbol{I}, \tag{9}$$

where $\boldsymbol{\Phi}_{p,q}^{(b)} = \mathrm{Diag}[e^{-j\beta_{p,q}^1}, e^{-j\beta_{p,q}^2}, \ldots, e^{-j\beta_{p,q}^K}]$ with $\beta_{p,q}^k = \frac{2\pi}{\lambda}[((N_x-1)d + 2pl)\mu_k + ((N_y-1)d + 2ql)\nu_k]$. Note that the backward signal vector is $\boldsymbol{x}_{p,q}^{(b)}(t) = \boldsymbol{A}\boldsymbol{\Phi}_{p,q}\boldsymbol{\Phi}_{p,q}^{(b)}\boldsymbol{s}^*(t) = \boldsymbol{J}\boldsymbol{x}_{p,q}^*(t)$, which is the flipped-and-conjugated version of $\boldsymbol{x}_{p,q}(t)$, with $\boldsymbol{J}$ the exchange matrix. As such, the backward smoothed covariance matrix becomes

$$\boldsymbol{R}^{(b)} = \frac{1}{PQ}\sum_{p=0}^{P-1}\sum_{q=0}^{Q-1}\boldsymbol{R}_{p,q}^{(b)} = \boldsymbol{A}\boldsymbol{M}^{(b)}\boldsymbol{A}^{\mathrm{H}}, \tag{10}$$

where

$$\boldsymbol{M}^{(b)} = \frac{\sigma_s^2}{PQ}\sum_{p=0}^{P-1}\sum_{q=0}^{Q-1}\boldsymbol{e}_{p,q}\boldsymbol{e}_{p,q}^{\mathrm{H}} = \frac{\sigma_s^2}{PQ}\boldsymbol{E}\boldsymbol{E}^{\mathrm{H}} \tag{11}$$

with $\boldsymbol{e}_{p,q} = \boldsymbol{\Phi}_{p,q}\boldsymbol{\Phi}_{p,q}^{(b)}\boldsymbol{\alpha}_{p,q}^{*}$ and $\boldsymbol{E} = [\boldsymbol{e}_{0,0}, \boldsymbol{e}_{0,1}, \ldots, \boldsymbol{e}_{P,Q}] \in \mathbb{C}^{K\times PQ}$. Averaging the forward and backward smoothed matrices renders the forward-backward smoothed covariance matrix as

$$\boldsymbol{R} = \frac{1}{2}\left(\boldsymbol{R}^{(f)} + \boldsymbol{R}^{(b)}\right) = \boldsymbol{A}\boldsymbol{M}\boldsymbol{A}^{\mathrm{H}}, \tag{12}$$

where $\boldsymbol{M} = \frac{1}{2}(\boldsymbol{M}^{(f)} + \boldsymbol{M}^{(b)}) = \frac{\sigma_s^2}{2PQ}[\boldsymbol{C}\ \boldsymbol{E}][\boldsymbol{C}\ \boldsymbol{E}]^{\mathrm{H}}$.

IV. Analysis of Degrees of Freedom

A. Number of Degrees of Freedom With Number of Movements

We first depict that, for a fixed $\boldsymbol{\alpha}$ across movement steps, both $\boldsymbol{C}$ and $\boldsymbol{E}$ have rank $\min(K, PQ)$. We then show that this rank conclusion holds when $\boldsymbol{\alpha}$ varies, and analyze the specific conditions that can lead to rank loss. Rewrite $\boldsymbol{C}$ as

$$\boldsymbol{C} = \mathrm{Diag}(\boldsymbol{\alpha})\ [\boldsymbol{\phi}_{0,0}\ \boldsymbol{\phi}_{0,1}, \ldots, \boldsymbol{\phi}_{P,Q}] = \boldsymbol{D}\boldsymbol{V}, \tag{13}$$

where $\boldsymbol{D}$ is a diagonal matrix with all non-zero entries and is thus full rank, and $\boldsymbol{V} = [\boldsymbol{\phi}_{0,0},\ \boldsymbol{\phi}_{0,1}, \ldots, \boldsymbol{\phi}_{P,Q}]$ is of rank $\min(K, PQ)$ due to its Vandermonde-like structure. Therefore, $\mathrm{rank}(\boldsymbol{C}) = \mathrm{rank}(\boldsymbol{V}) = \min(\mathrm{K}, \mathrm{PQ})$. Similarly, rewrite $\boldsymbol{E}$ as

$$\boldsymbol{E} = \mathrm{Diag}(\boldsymbol{\Phi}_{p,q}^{(b)}\boldsymbol{\alpha}^{*})\ [\boldsymbol{\phi}_{0,0}\ \boldsymbol{\phi}_{0,1}, \ldots, \boldsymbol{\phi}_{P,Q}] = \boldsymbol{G}\boldsymbol{V}, \tag{14}$$

where $\boldsymbol{G}$ is diagonal and thus full rank. Therefore, $\mathrm{rank}(\boldsymbol{E}) = \mathrm{rank}(\boldsymbol{V}) = \min(K, PQ)$. From Eqs. (12)–(14), $\boldsymbol{M} = [\boldsymbol{D}\boldsymbol{V}\ \ \boldsymbol{G}\boldsymbol{V}] \in \mathbb{C}^{K\times 2PQ}$ and its rank is $\min(K, 2PQ)$. Therefore, when using the forward-backward smoothed matrix $\boldsymbol{R}$, detecting K coherent signals requires $K \le 2PQ$. Furthermore, for a subspace-based algorithm, such as MUSIC, to detect K coherent signals using the URA, the number of achievable DOFs is $N_xN_y - 1$, provided that at least

$$PQ \ge \frac{N_xN_y - 1}{2} \tag{15}$$

steps of movement are performed.

Now we consider the case where the vector $\boldsymbol{\alpha}$ varies across moving steps, with each instance drawn from a random distribution.

Lemma 1: For any $H < \min(K, PQ)$, $\mathrm{rank}(\boldsymbol{C}) \le \mathrm{H}$ holds if only if $\boldsymbol{C}$ has the form $\boldsymbol{C} = \boldsymbol{U}\boldsymbol{F}$ or equivalently

$$\boldsymbol{c}_m = \sum_{h}^{H}\boldsymbol{u}^{(h)}\boldsymbol{f}_m^{(h)} \tag{16}$$

for $m \in \{1, 2, \ldots, PQ\}$, where $\boldsymbol{U} = [\boldsymbol{u}^{(1)}, \ldots, \boldsymbol{u}^{(H)}] \in \mathbb{C}^{K\times H}$ and $\boldsymbol{F} = [\boldsymbol{f}_1, \ldots, \boldsymbol{f}_{PQ}] \in \mathbb{C}^{H\times PQ}$.

Proof: If $\boldsymbol{C} = \boldsymbol{U}\boldsymbol{F}$, then $\mathrm{rank}(\boldsymbol{C}) \le \min(\mathrm{rank}(\boldsymbol{U}), \mathrm{rank}(\boldsymbol{F})) \le \mathrm{H}$. Conversely, if $\mathrm{rank}(\boldsymbol{C}) \le \mathrm{H}$, then all columns $\boldsymbol{c}_m$ lie in an H-dimensional subspace. Choosing a basis $\boldsymbol{U}$ for this subspace yields $\boldsymbol{c}_m = \boldsymbol{U}\boldsymbol{f}_m$ and hence $\boldsymbol{C} = \boldsymbol{U}\boldsymbol{F}$. □

By this lemma, the rank of $\boldsymbol{C}$ becomes smaller than $\min(K, PQ)$ only if $\alpha_{k,m} = [\boldsymbol{U}\boldsymbol{f}_m]_k/[\boldsymbol{\phi}_m]_k$, which is the kth entry at the mth moving step for fixed matrix $\boldsymbol{U}$. Since $\boldsymbol{\alpha}_m$ is drawn independently of $\boldsymbol{\phi}_m$, such case occurs with a negligible probability. Therefore, we have $\mathrm{rank}(\boldsymbol{C}) = \min(\mathrm{K}, \mathrm{PQ})$ and, similarly, $\mathrm{rank}(\boldsymbol{E}) = \min(\mathrm{K}, \mathrm{PQ})$.

B. Numerical Rank Loss for Small Movement

Although the theoretical rank of $\boldsymbol{V}$ is $\min(K, PQ)$ for any $l \neq 0$, in practice, small l values may lead to numerical rank deficiency due to limited phase variations across columns. Similar observations are reported in [30], [31], where the effect of inter-element spacing is analyzed in massive MIMO systems. When the spacing is at least half wavelength, communication channels remain largely uncorrelated, whereas smaller spacings increase spatial correlation and reduced channel rank. This behavior is analogous to the numerical rank loss observed here when l is small.

To illustrate the effect, we consider an extreme case with forward smoothing only. The rank of the smoothed covariance matrix $\boldsymbol{R}^{(f)}$ is determined by the rank of the matrix $\boldsymbol{C}$. Since each column is given by $\boldsymbol{c}_{p,q} = \boldsymbol{\Phi}_{p,q}\boldsymbol{\alpha}$, it follows that $\boldsymbol{c}_{0,0} = \boldsymbol{\alpha}$. We define $\boldsymbol{c}_{p,q} = \boldsymbol{c}_{0,0} + \Delta_{p,q}$, where $\Delta_{p,q} = (\boldsymbol{\Phi}_{p,q} - \boldsymbol{I})\boldsymbol{\alpha}$. Thus, the matrix $\boldsymbol{C}$ can be expressed as

$$\boldsymbol{C} = [\boldsymbol{c}_{0,0},\ \boldsymbol{c}_{0,0} + \Delta_{0,1},\ \cdots,\ \boldsymbol{c}_{0,0} + \Delta_{P,Q}]. \tag{17}$$

As $l \to 0$, we have $\boldsymbol{\Phi}_{p,q} \to \boldsymbol{I}$, i.e., $\Delta_{p,q} \approx \boldsymbol{0}$. In this limiting case, all columns of $\boldsymbol{C}$ converge to $\boldsymbol{c}_{0,0}$, and the matrix becomes rank one. For small but nonzero values values of l, the terms $\Delta_{p,q}$ remains small, making the columns of $\boldsymbol{C}$ to be nearly identical and resulting in numerical rank deficiency. Although we consider a fixed displacement l per movement, the rank conclusions depend only on the set of distinct array placements, not on uniform spacing. As long as l is adequately large, varying l across steps still preserves the rank of $\boldsymbol{V}$.

C. Impact of the Motion Support

The motion support of the array across the X and Y axes plays an important role in the decorrelation performance. Specifically, if all PQ movement steps are confined to a single axis, e.g., the X axis, each element of $\boldsymbol{V}$, which includes the phase term γ, depends only on μ and not on ν. As a result, rows of $\boldsymbol{V}$ corresponding to identical μ values become identical, resulting in rank deficiency. Each pair of identical rows reduces the rank of $\boldsymbol{V}$ by one. Although forward-backward smoothing via the concatenated matrix $\boldsymbol{F} = [\boldsymbol{C}\ \boldsymbol{E}]$ can recover one rank, enabling resolution of up to two signals with the same μ, it cannot resolve more than two such signals under single-axis motion. Even when the μ values are not exactly equal but take close values, one-dimensional motion still suffers from reduced decorrelation capability. As the number of signals increases, the likelihood of having such closely spaced μ values also increases, exacerbating performance degradation under single-axis movement. In contrast, a balanced (P, Q) motion support introduces variations along both μ and ν, ensuring that rows of $\boldsymbol{V}$ remain distinguishable even when multiple signals share the same μ values, as long as their ν values differ.

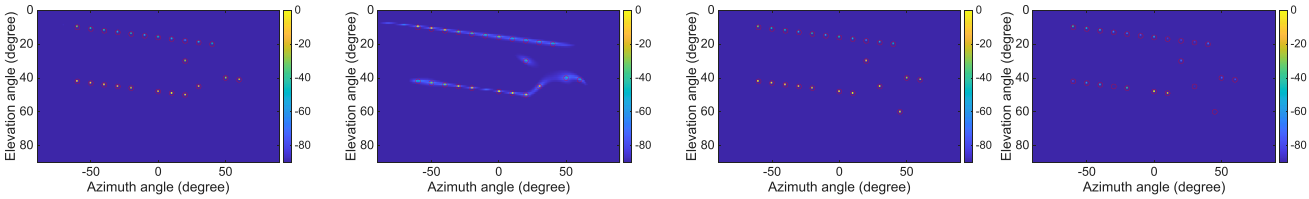

(a) Scenario 1, $(P, Q) = (4, 3)$ (b) Scenario 1, $(P, Q) = (12, 1)$ (c) Scenario 2, $(P, Q) = (4, 3)$ (d) Scenario 2, $(P, Q) = (12, 1)$

Fig. 2. DOA estimation performance with different motion support.

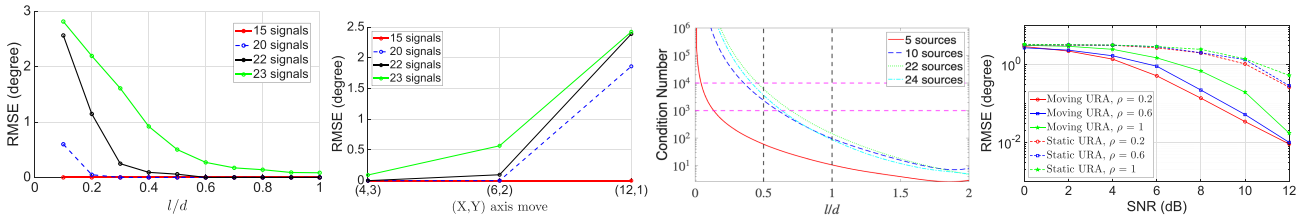

(a) RMSE versus l (b) RMSE versus motion support (c) $\mathrm{cond}(\boldsymbol{V})$ versus l (d) RMSE versus input SNR

Fig. 3. Performance comparison.

V. Simulation Results

Consider a 25-element URA with $N_x = 5$ and $N_y = 5$. The maximum number of DOFs is $N_x N_y - 1 = 24$, compared with 11 for the static URA. The magnitudes of the attenuation factors $\boldsymbol{\alpha}$ are drawn from a uniform distribution between 0.5 and 2, and the phases are uniformly selected between 30° and 60°. To decorrelate the covariance matrix using the forward-backward smoothing strategy, 12 array movement steps are required according to (15). Fig. 2 depicts the DOA estimation performance for two scenarios, each consisting of $K = 23$ coherent signals, which closely approaches the array DOFs. Among them, we consider two azimuth–elevation pairs that result in the same μ value $\mu = 0.6124$, which are $(-30^\circ, 45^\circ)$ and $(30^\circ, 45^\circ)$. Fig. 2(a) and (b) illustrate that both motion supports, i.e., (X axis movement, Y axis movement) = (4,3) and (12,1), successfully detect all 23 signals, although the (4,3) support yields a much cleaner spectrum due to 2D phase variation. In each step, the array is displaced by $l = d$. A total of 100 noise-free snapshots is used. Note that true DOAs are shown as red circles and the estimated spectrum is normalized and is shown in dB scale. In the second scenario, we include another DOA pair with the same $\mu = 0.6124$, which is $(45^\circ, 60^\circ)$, so that the three pairs $(-30^\circ, 45^\circ)$, $(30^\circ, 45^\circ)$, and $(45^\circ, 60^\circ)$ share the same μ. As shown in Fig. 2(c) and (d), while the (4,3) motion support continues to detect all signals, the (12,1) support fails to detect the three signals corresponding to equal μ value.

Fig. 3(a) and (b) show the root-mean-squared-error (RMSE) performance of the estimated DOAs against the displacement l per movement step and the movement pattern, respectively. The input SNR of the reference signal is set to 10 dB, and 100 snapshots are used. It is observed in Fig. 3(a) that, for $l = d$, the RMSE remains low across all scenarios, even when the number of sources approaches the DOF limit, indicating that $l \geq d$ is sufficient for effective decorrelation. For a smaller number of sources (e.g., 15, 20, and 22), a lower displacement (e.g., $l = 0.5$ d) still performs well, choosing $l = d$ consistently yields lower RMSE across all cases. To further illustrates the impact of l, Fig. 3(c) shows the condition number of matrix $\boldsymbol{V}$ versus l. It is observed that small l values produce high condition numbers. As l increases, inter-row correlation and, correspondingly, the condition number decrease. At $l = d = \lambda/2$, the condition number falls below 10^3, which is commonly regarded as well-conditioned, whereas $10^3 - 10^4$ is moderately well-conditioned [32]. For $l = 0.5$ d, the condition number lies in the moderately well-conditioned range, which still preserves the rank of $\boldsymbol{V}$ but may yield lower accuracy compared with the $l = d$ case. Although the condition number may exhibit periodic peaks at specific l values, these occur only at points requiring high numerical precision and are negligible on practical l grids.

It is observed in Fig. 3(b) that, for a high number of signals, the performance of the one-dimensional motion support degrades because the μ values are more closely spaced. In contrast, balanced 2D motions result in lower RMSE values due to richer phase variation across both dimensions.

Fig. 3(d) compares the RMSE versus input SNR for static and moving URAs across various correlation coefficients ρ, considering 2 coherent sources. The moving-array scheme consistently outperforms the static array at all SNR levels by fully exploiting the entire array aperture during smoothing.

VI. Conclusion

This letter proposed a moving array-based decorrelation strategy for 2D DOA estimation of coherent signals to achieve increased DOFs compared to the static array case. We derived the required number of movement steps necessary to attain the full DOFs. The impact of the motion support was analyzed, and it was demonstrated that balanced 2D motion provides stronger decorrelation capability than purely one-dimensional movement. Finally, we showed that full decorrelation and maximum DOFs can be achieved as long as the array moves by at least half the wavelength of the impinging signal in each step. Simulation results confirmed the effectiveness of the proposed approach.

REFERENCES

[1] D. H. Johnson, *Array Signal Processing: Concepts and Techniques*. Englewood Cliffs, NJ, USA: Prentice-Hall, 1993.

[2] H. L. V. Trees, *Optimum Array Processing: Part IV of Detection, Estimation, and Modulation Theory*. Hoboken, NJ, USA: Wiley, 2002.

[3] T. E. Tuncer and B. Friedlander, *Classical and Modern Direction-of-Arrival Estimation*. Orlando, FL, USA: Academic Press, 2009.

[4] M. G. Amin, X. Wang, Y. D. Zhang, F. Ahmad, and E. Aboutanios, "Sparse array and sampling for interference mitigation and DOA estimation in GNSS," *Proc. IEEE*, vol. 104, no. 6, pp. 1302–1317, Jun. 2016.

[5] S. Sun, A. P. Petropulu, and H. V. Poor, "MIMO radar for advanced driver-assistance systems and autonomous driving: Advantages and challenges," *IEEE Signal Process. Mag.*, vol. 37, no. 4, pp. 98–117, Jul. 2020.

[6] S. Sun and Y. D. Zhang, "4D automotive radar sensing for autonomous vehicles: A sparsity-oriented approach," *IEEE J. Sel. Topics Signal Process.*, vol. 15, no. 4, pp. 879–891, Jun. 2021.

[7] W. Liu, M. Haardt, M. S. Greco, C. F. Mecklenbräuker, and P. Willett, "Twenty-five years of sensor array and multichannel signal processing: A review of progress to date and potential research directions," *IEEE Signal Process. Mag.*, vol. 40, no. 4, pp. 80–91, Jun. 2023.

[8] R. Schmidt, "Multiple emitter location and signal parameter estimation," *IEEE Trans. Antennas Propag.*, vol. AP-34, no. 3, pp. 276–280, Mar. 1986.

[9] R. Roy and T. Kailath, "ESPRIT–Estimation of signal parameters via rotational invariance techniques," *IEEE Trans. Acoust. Speech Signal Process.*, vol. 37, no. 7, pp. 984–995, Jul. 1989.

[10] J. E. Evans, J. R. Johnson, and D. Sun, "Application of advanced signal processing techniques to angle of arrival estimation in ATC navigation and surveillance systems," MIT Lincoln Lab., Cambridge, MA, USA, Tech. Rep. 582, 1982.

[11] T.-J. Shan, M. Wax, and T. Kailath, "On spatial smoothing for direction-of-arrival estimation of coherent signals," *IEEE Trans. Acoust., Speech, Signal Process.*, vol. ASSP-33, no. 4, pp. 806–811, Aug. 1985.

[12] B. Friedlander and A. Weiss, "Direction finding using spatial smoothing with interpolated arrays," *IEEE Trans. Aerosp. Electron. Syst.*, vol. 28, no. 2, pp. 574–587, Apr. 1992.

[13] C.-L. Liu and P. Vaidyanathan, "Remarks on the spatial smoothing step in coarray MUSIC," *IEEE Signal Process. Lett.*, vol. 22, no. 9, pp. 1438–1442, Sep. 2015.

[14] H. Zheng, C. Zhou, Z. Shi, and Y. Gu, "Structured tensor reconstruction for coherent DOA estimation," *IEEE Signal Process. Lett.*, vol. 29, pp. 1634–1638, 2022.

[15] S. R. Pavel, Y. D. Zhang, S. Sun, and A. L. D. Almeida, "Tensor reconstruction-based sparse array 2-D DOA estimation of mixed coherent and uncorrelated signals," in *Proc. IEEE Int. Conf. Acoust., Speech, Signal Process.*, 2024, pp. 12876–12880.

[16] S. U. Pillai and B. H. Kwon, "Forward/backward spatial smoothing techniques for coherent signal identification," *IEEE Trans. Acoust., Speech, Signal Process.*, vol. 37, no. 1, pp. 8–15, Jan. 1989.

[17] F.-M. Han and X.-D. Zhang, "An ESPRIT-like algorithm for coherent DOA estimation," *IEEE Antennas Wireless Propagat. Lett.*, vol. 4, pp. 443–446, 2005.

[18] Y.-H. Choi, "ESPRIT-based coherent source localization with forward and backward vectors," *IEEE Trans. Signal Process.*, vol. 58, no. 12, pp. 6416–6420, Dec. 2010.

[19] S. R. Pavel and Y. D. Zhang, "Direction-of-arrival estimation of mixed coherent and uncorrelated signals," *IEEE Signal Process. Lett.*, vol. 31, pp. 2180–2184, 2024.

[20] Y.-M. Chen, "On spatial smoothing for two-dimensional direction-of-arrival estimation of coherent signals," *IEEE Trans. Signal Process.*, vol. 45, no. 7, pp. 1689–1696, Jul. 1997.

[21] H. Yi and X. Zhou, "On 2D forward-backward spatial smoothing for azimuth and elevation estimation of coherent signals," in *Proc. IEEE Antennas Propag. Soc. Int. Symp.*, 2005, vol. 2B, pp. 80–83.

[22] J. A. Fawcett, "Synthetic aperture processing for a towed array and a moving source," *J. Acoust. Soc. Amer., vol.* 94, no. 5, pp. 2832–2837, 1993.

[23] S. Kim, D. H. Youn, and C. Lee, "Temporal domain processing for a synthetic aperture array," *IEEE J. Ocean. Eng., vol.* 27, no. 2, pp. 322–327, Apr. 2002.

[24] G. Qin, Y. D. Zhang, and M. G. Amin, "DOA estimation exploiting moving dilated nested arrays," *IEEE Signal Process. Lett.*, vol. 26, no. 3, pp. 490–494, Mar. 2019.

[25] G. Qin, M. G. Amin, and Y. D. Zhang, "DOA estimation exploiting sparse array motions," *IEEE Trans. Signal Process.*, vol. 67, no. 11, pp. 3013–3027, Jun. 2019.

[26] J. Chu, Z. Zhang, Y. Huang, and T. Su, "Exploration on 2D DOA estimation of linear array motion: Uniform and sparse circular motion," *IEEE Trans. Signal Process.*, vol. 72, pp. 4115–4131, 2024.

[27] H. Wu, Q. Shen, W. Cui, and W. Liu, "DOA estimation with nonuniform moving sampling scheme based on a moving platform," *IEEE Signal Process. Lett.*, vol. 28, pp. 1714–1718, 2021.

[28] L. Liu, S. Liu, Y. Huang, and M. G. Amin, "Joint DoA-range estimation using moving time-modulated frequency diverse coprime array," in *Proc. IEEE Radar Conf.*, 2022, pp. 1–6.

[29] W. Li, X. Xu, X. Huang, and Y. Yang, "Direction-of-arrival estimation for coherent signals exploiting moving coprime array," *IEEE Signal Process. Lett.*, vol. 30, pp. 304–308, 2023.

[30] C. Masouros and M. Matthaiou, "Space-constrained massive MIMO: Hitting the wall of favorable propagation," *IEEE Commun. Lett.*, vol. 19, no. 5, pp. 771–774, May 2015.

[31] J. Zhang, L. Dai, M. Matthaiou, C. Masouros, and S. Jin, "On the spectral efficiency of space-constrained massive mimo with linear receivers," in *Proc. IEEE Int. Conf. Commun.*, 2016, pp. 1–6.

[32] L. N. Trefethen and D. Bau, *Numerical Linear Algebra*. Philadelphia, PA, USA: SIAM, 2022.